Coloring Ultra-sensitive MRI by Tunable Metal-Organic Frameworks

Yuqi Yang,[a,b] Yingfeng Zhang,[a] Baolong Wang,[a] Qianni Guo,[a,b] Yaping Yuan,[a,b] Weiping Jiang,[a,b] Lei Shi,[a,b] Minghui Yang,[a,b] Shizhen Chen,[a,b] Xin Lou,[c] Xin Zhou*[a,b]

[a] Key Laboratory of Magnetic Resonance in Biological Systems, State Key Laboratory of Magnetic Resonance and Atomic and Molecular Physics, National Center for Magnetic Resonance in Wuhan, Wuhan Institute of Physics and Mathematics, Innovation Academy for Precision Measurement Science and Technology, Chinese Academy of Sciences-Wuhan National Laboratory for Optoelectronics, Wuhan 430071, China. Email: xinzhou@wipm.ac.cn.

[b] University of Chinese Academy of Sciences, Beijing 100049, China

[c] Department of Radiology, Chinese PLA General Hospital, Beijing 100039, China

Section S1

Preparation of IRMOFs

Materials and Instruments

All chemicals were commercially obtained and used without further purification. 1,4-benzenedicarboxylic acid (H_2BDC), 2,6-Naphthalenedicarboxylic acid (2,6-NDC) and Biphenyl-4,4'-dicarboxylic acid (BPDC) were purchased from J&K Chemicals. $Zn(NO_3)_2 \cdot 6H_2O$ and KBr (99.99%) were purchased from Aladdin (Shanghai, 99.99%). Polyvinyl pyrrolidone (PVP, Mw 30000), N, N-dimethylformamide (DMF, AR) and ethanol (AR) were obtained from Sinopharm Chemical Reagent Co., Ltd (Shanghai, China).

The synthesized nanoparticles were characterized by transmission electron microscopy (TEM, JEM-2100), high resolution transmission electron microscopy (HTEM, Tecnai G2 F20 U-TWIN), field emission scanning electron microscope (SEM, ZEISS GeminiSEM 500), dynamic light scattering (Malvern Panalytical, Zetasizer Nano ZS), powder X-ray Diffraction (PXRD), N_2 adsorption analysis (BELSORP-max), Fourier Transform infrared spectroscopy (FTIR, Thermo Scientific Nicolet iS10). ^{129}Xe NMR and ^{129}Xe MRI experiments were carried out using a 400 MHz Bruker AV400 wide-bore spectrometer (Bruker Biospin, Ettlingen, Germany).

Synthesis procedures

According to the former studies,[1-4] MOF spheres could be prepared by a simple hydrothermal approach: Briefly, 5 mg H_2BDC (0.03 mM), 24 mg $Zn(NO_3)_2 \cdot 6H_2O$ (0.08 mM) and 312 mg PVP were dissolved in 13.3 mL DMF-ethanol mixed solution (v:v = 5:3) under stirring and then dispersed under sonication for 20 min. The resulting mixture was transferred to a Teflon-lined stainless-steel autoclave (25 mL) and heated at 150℃ for 12 h. After gently cooling down to room temperature, the solution was centrifuged at 10000 rpm for 15 min, and the bottom white solid was further washed with DMF and ethanol for 3 times, respectively. The produced nanopaticles were dispersed in ethanol for further use. The produced nanoparticles

were known as IRMOF-1, where "I" means "isoreticular", and "R" is "reticular".[5]

IRMOF-8 and IRMOF-10 nanospheres were synthesized by the similar procedures as IRMOF-1, which only replaced the H_2BDC to 0.03 mM 2,6-NDC (6.5 mg) or BPDC (7.3 mg).

Section S2

Hyper-CEST MR procedures

Hyper-CEST ^{129}Xe NMR

Hyperpolarized ^{129}Xe gas was produced by a home-built ^{129}Xe hyperpolarizer. The ^{129}Xe polarization was about 10%. A gas mixture of 10% N_2, 88% He, and 2% Xe (natural abundant ^{129}Xe) was flowed through a home-made hyperpolarizer (hyperpolarized^{129}Xe nuclear spin polarization was 100,000 times greater than its thermal equilibrium polarization), the resulting gas was guided to the NMR spectrometer and directly bubbled into the MOF dispersed solution at a flow rate of 100 mL/min for 20 s. After a 3s delay allowing the bubbles collapse, continuous wave (CW) pulses were applied to selectively saturate the Xe@MOF cage peak (10 s with a 6.0 μT field). This was followed by the acquisition of a spectrum. Each spectrum was acquired in a single scan. NMR spectra for CEST were processed using 6 Hz line broadening filter. The aqueous ^{129}Xe signal was defined as 0 ppm. Saturation contrast represents the normalized difference between on-resonance and off-resonance signals.

Hyper-CEST ^{129}Xe MRI

^{129}Xe MRI was generated with RARE sequence with eight-echo trains and 4.6 ms effective echo time. Including bubbling, wait and saturation times, the overall repetition time (TR) was 28 seconds. All images were axial without slice selection, and the k-space matrix comprised 32 points in the readout dimension and 32 phase-encoding points. The field of view was 20 mm by 20 mm. The 32×32 image was interpolated into 64×64 image matix, and the CEST effect was calculated using (Soff-Son)/Soff，where Soff indicated the average image signal intensity of off-resonance saturation and Son indicated the average image signal intensity of on-resonance saturation. The CEST contrast map was then median filter using 3×3 sample window and segmented by threshold.

Section S3

Morphology characterization

Scanning Electron Microscopy (SEM) imaging of IRMOFs

The produced IRMOF-1, IRMOF-8 and IRMOF-10 were dispersed in ethanol respectively. After sonication for 5 minutes, 20 μL of the dispersion was dropped onto a semiconductor silicon wafer and dried in air. SEM was performed with accelerating voltage of 20.00 kV.

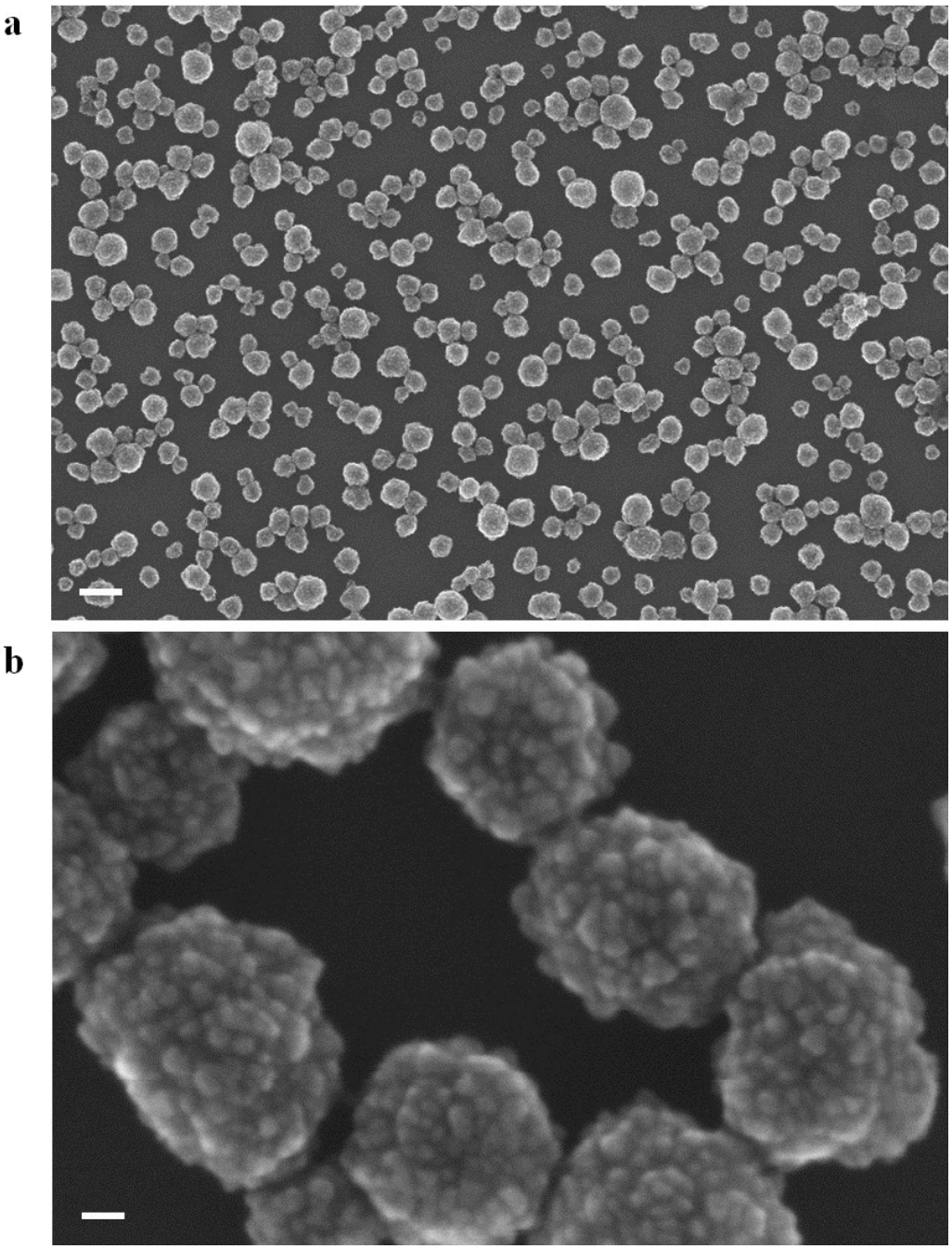

Figure S1. SEM image of IRMOF-1 nanoparticles. Scar bar, a) 200 nm, b) 20 nm.

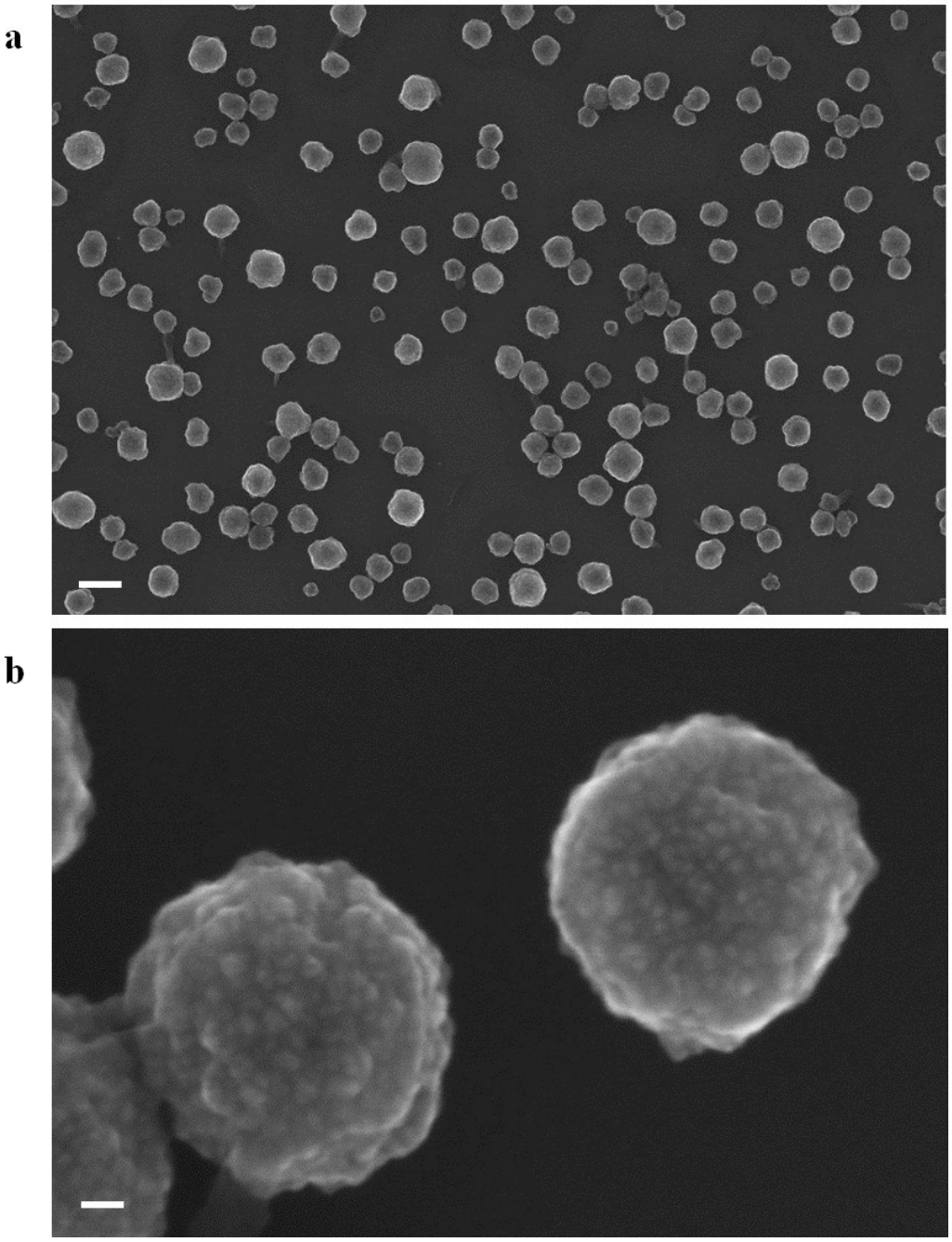

Figure S2. SEM image of IRMOF-8 nanoparticles. Scar bar, a) 200 nm, b) 20 nm.

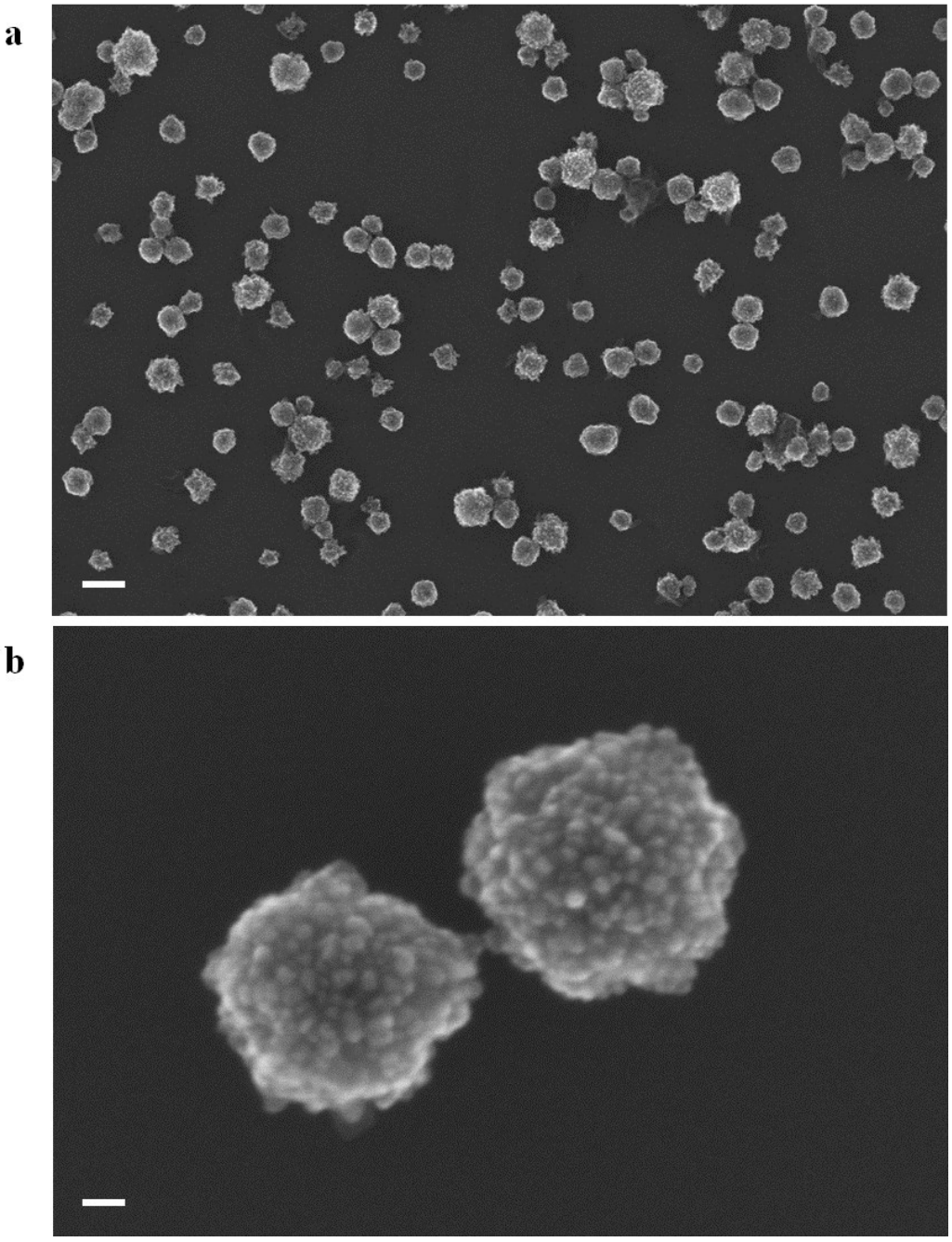

Figure S3. SEM image of IRMOF-10 nanoparticles. Scar bar, a) 200 nm, b) 20 nm.

Transmission electron microscopy (TEM) and high resolution transmission electron microscopy (HTEM) images of IRMOFs

IRMOF-1, IRMOF-8, IRMOF-10 nanoparticles were dispersed in ethanol at a concentration of 0.2 mg/mL respectively. After sonication for 5 minutes, 10 μL of the IRMOF in ethanol dispersion was dropped onto a copper grid and dried in air. TEM images were obtained on a JEOL JEM-2100 microscope.

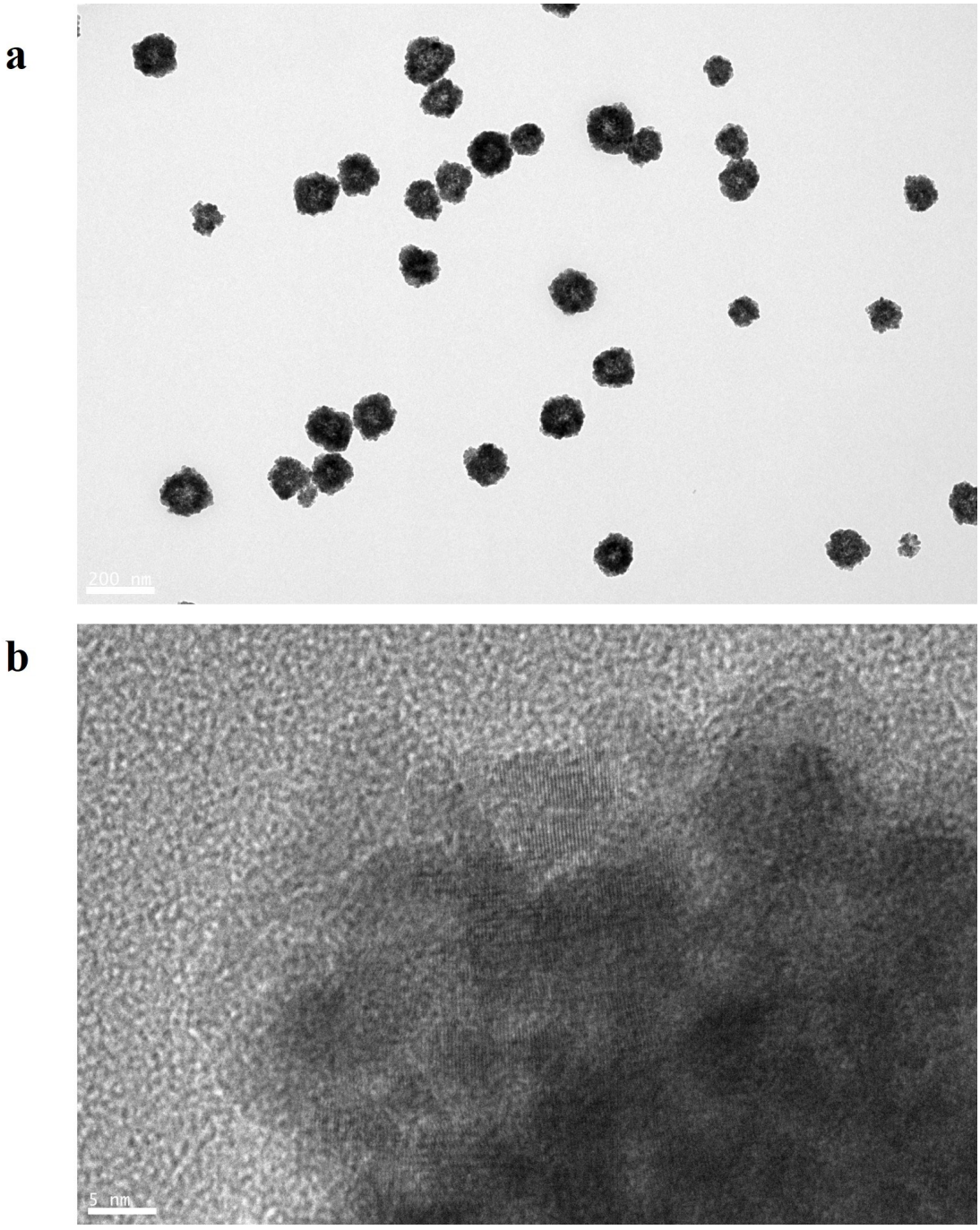

Figure S4. TEM a) and HTEM b) image of IRMOF-1 nanoparticles. Scar bar, a) 200 nm, b) 5 nm.

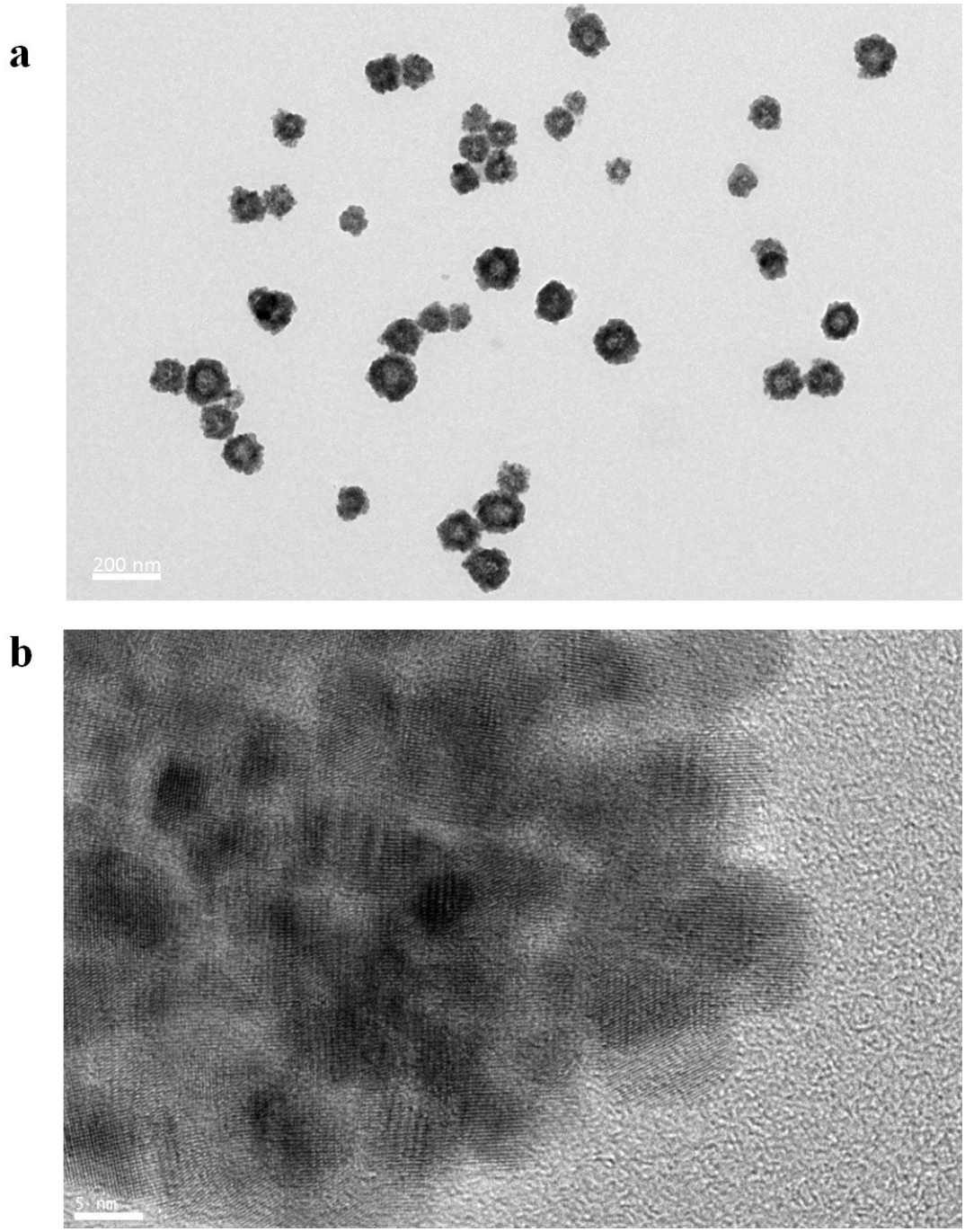

Figure S5. TEM a) and HTEM b) image of IRMOF-8 nanoparticles. Scar bar, a) 200 nm, b) 5 nm.

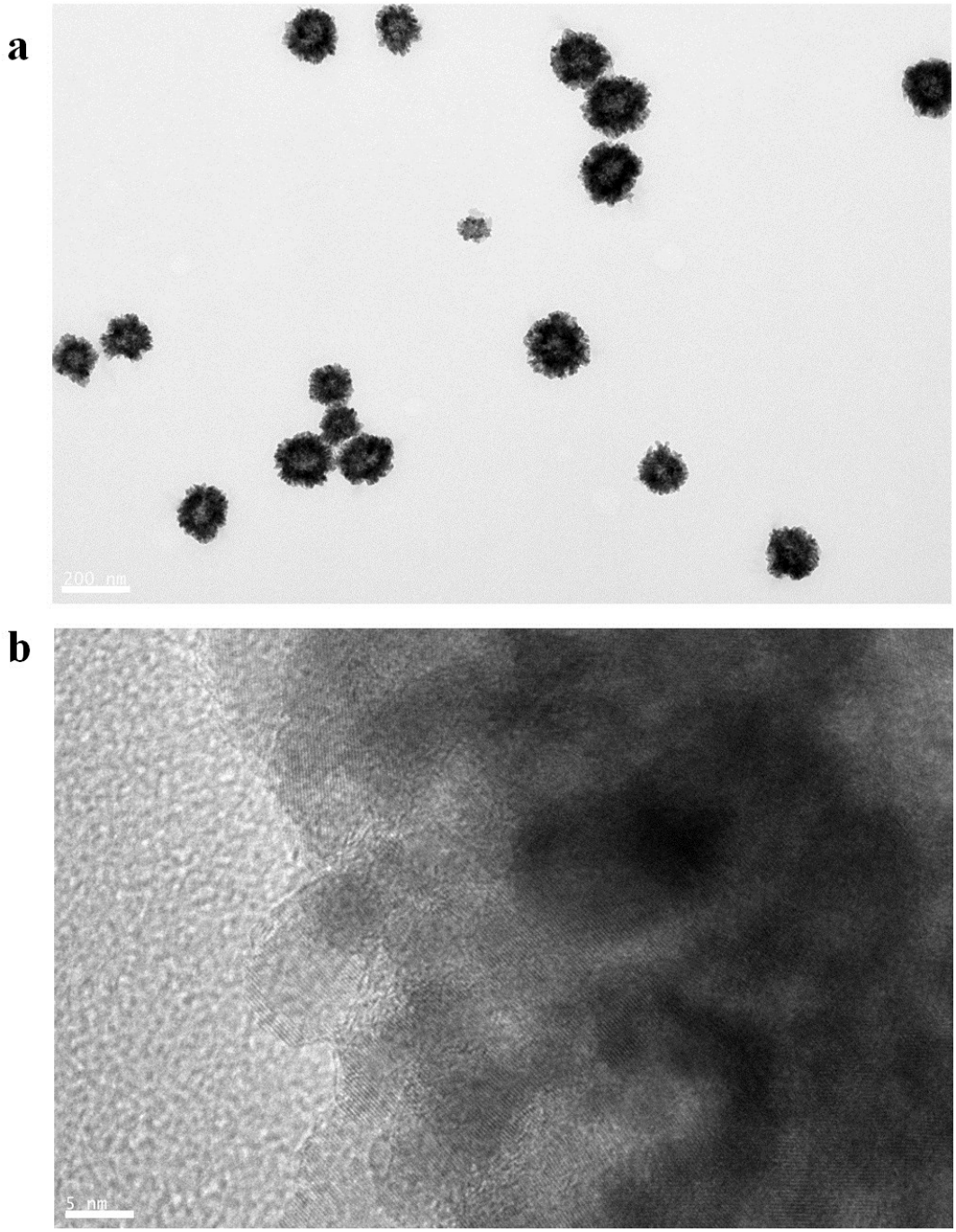

Figure S6. TEM a) and HTEM b) image of IRMOF-10 nanoparticles. Scar bar, a) 200 nm, b) 5 nm.

Section S4

Particle size analysis

Particle size counted by TEM

The diameter of IRMOF nanoparticles were counted by image analysis software, SigmaScan. Three TEM images with the same magnification in different visual field were imported into SigmaScan, and the dimeter were measured respectively. The results were analyzed by Origin to calculate the size distribution, average diameter and relative average deviation.

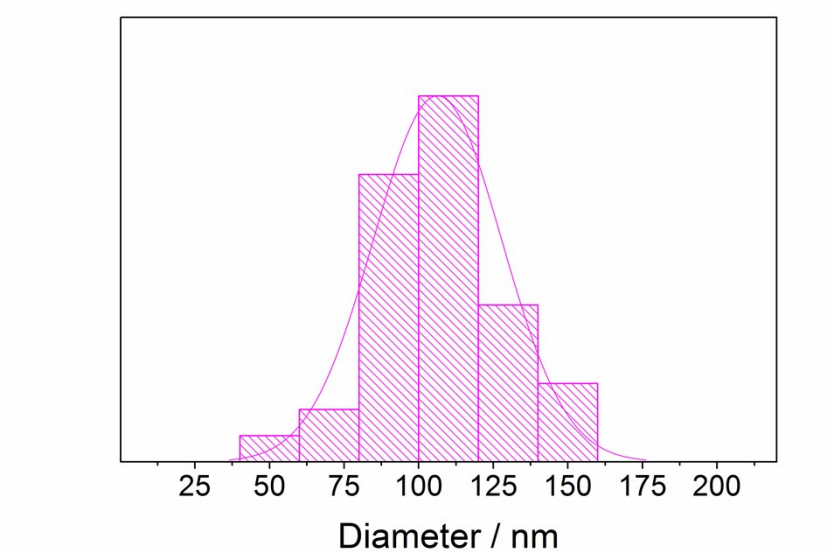

Figure S7. Size distribution of IRMOF-1 nanoparticles in TEM images.

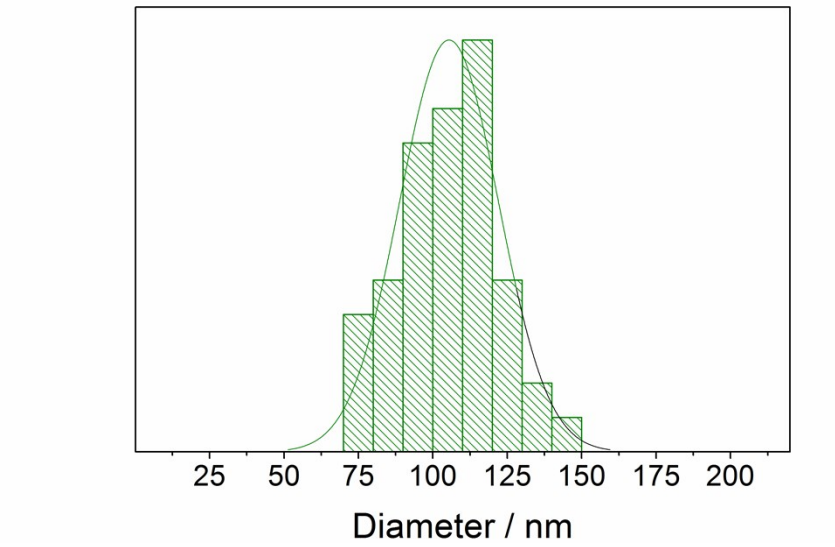

Figure S8. Size distribution of IRMOF-8 nanoparticles in TEM images.

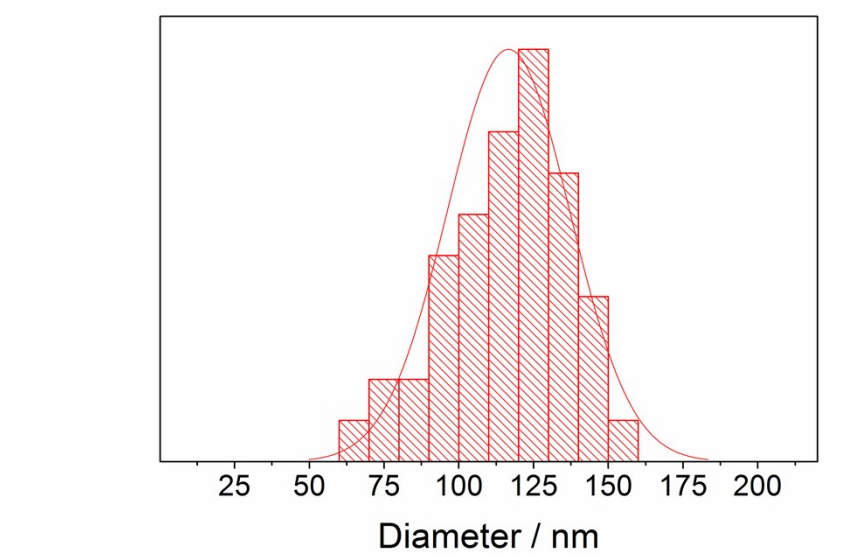

Figure S9. Size distribution of IRMOF-10 nanoparticles in TEM images.

	Average diameter (nm)	Relative Average Deviation
IRMOF-1	106.3	0.202
IRMOF-8	105.2	0.157
IRMOF-10	116.6	0.176

Table S1. Particle size distribution counted by TEM images. The average diameters of the IRMOF nanoparticles were ranging from 105 nm to 116 nm.

DLS analysis

The produced IRMOF-1, IRMOF-8 and IRMOF-10 were dispersed in ultra-pure water respectively and sonicated for 10 minutes before use.

Results showed the diameter of the prepared nanoparticles were around 100 nm with low PDI values, indicating uniform sizes for nano-sized ZIF-8.

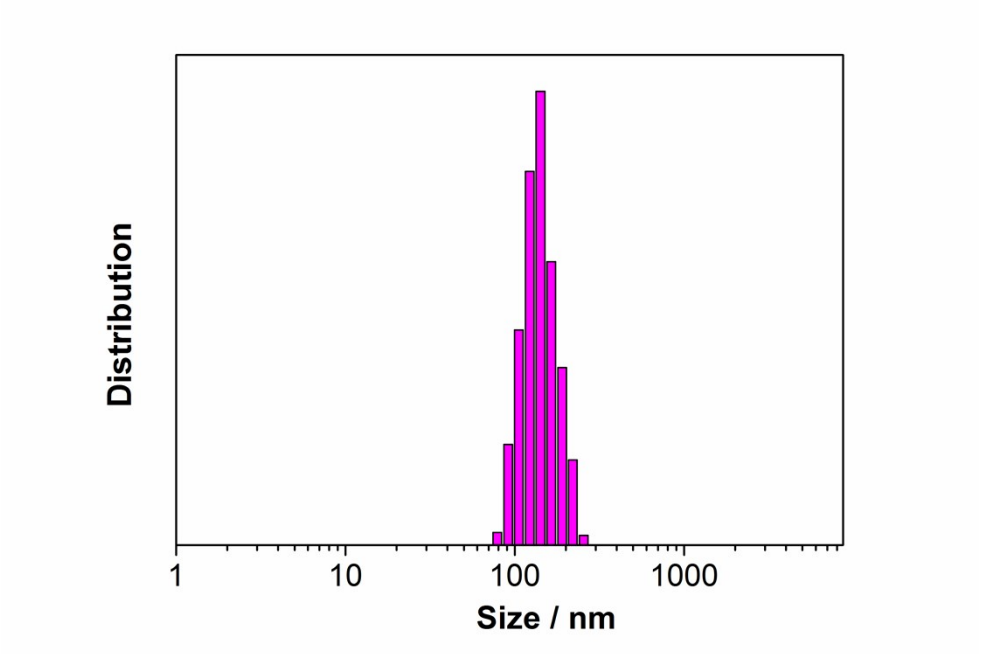

Figure S10. DLS size distribution of IRMOF-1 nanoparticles in water dispersion.

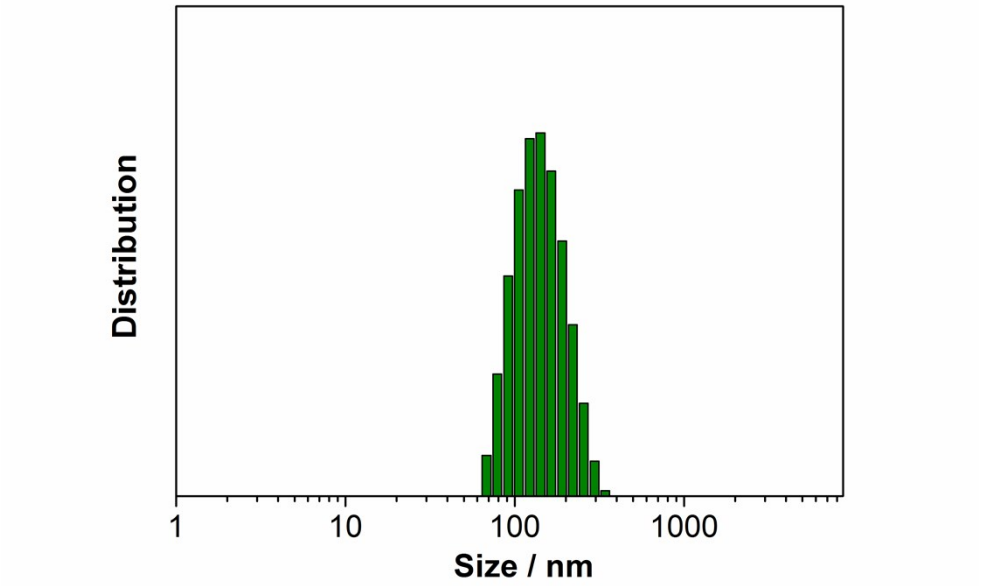

Figure S11. DLS size distribution of IRMOF-8 nanoparticles in water dispersion.

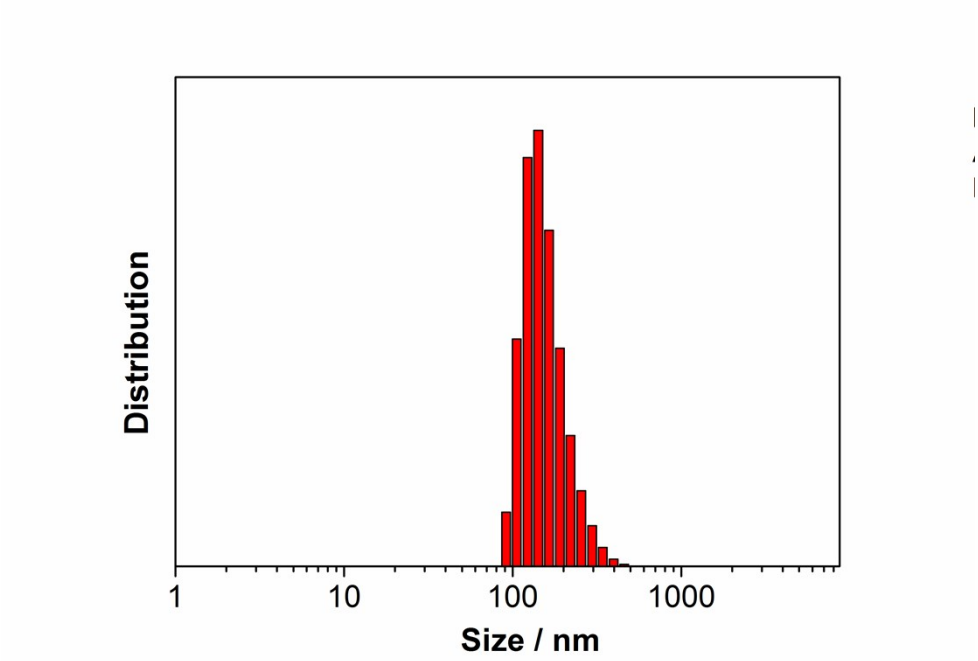

Figure S12. DLS size distribution of IRMOF-10 nanoparticles in water dispersion.

	Hydrodynamic diameter in H_2O (nm)	PDI
IRMOF-1	149.9	0.163
IRMOF-8	146.3	0.131
IRMOF-10	157.5	0.207

Table S2. Particle size distribution analysis. Based on the dynamic light scattering (DLS) results, the hydrodynamic diameter of IRMOF-1, IRMOF-8 and IRMOF-10 were around 150 nm. The IRMOFs exhibited a uniform size distribution according to the low PDI values.

Section S5

X-ray ***Diffraction***

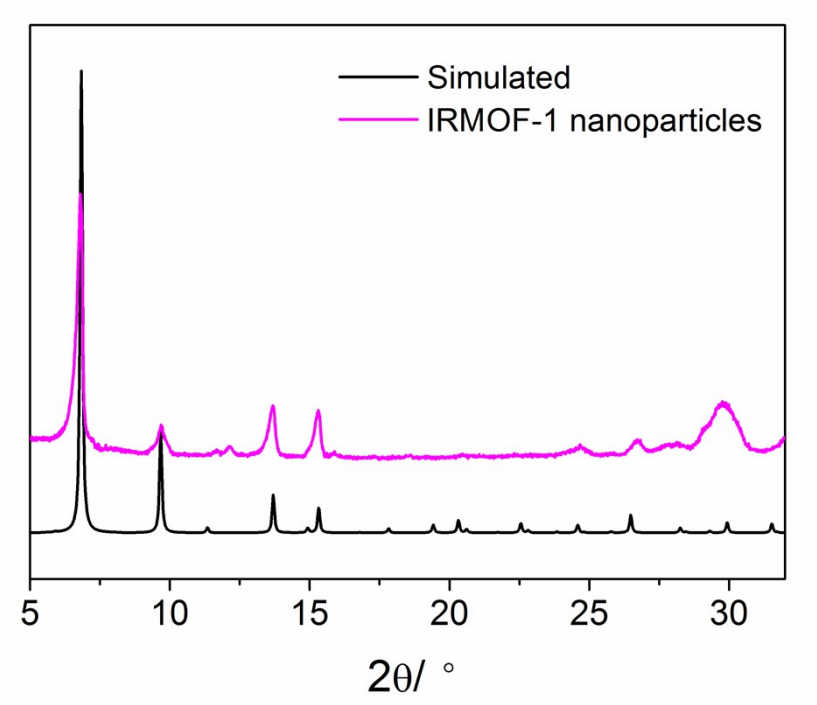

Figure S13. Comparisons of the PXRD patterns of synthesized IRMOF-1 nanoparticles with the simulated diffraction pattern.

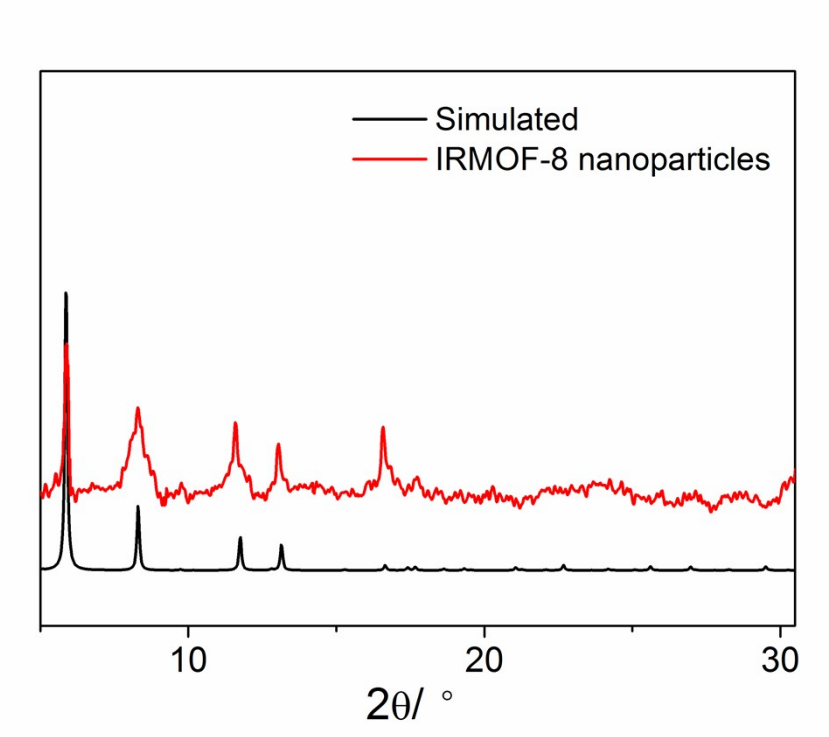

Figure S14. Comparisons of the PXRD patterns of synthesized IRMOF-8 nanoparticles with the simulated diffraction pattern.

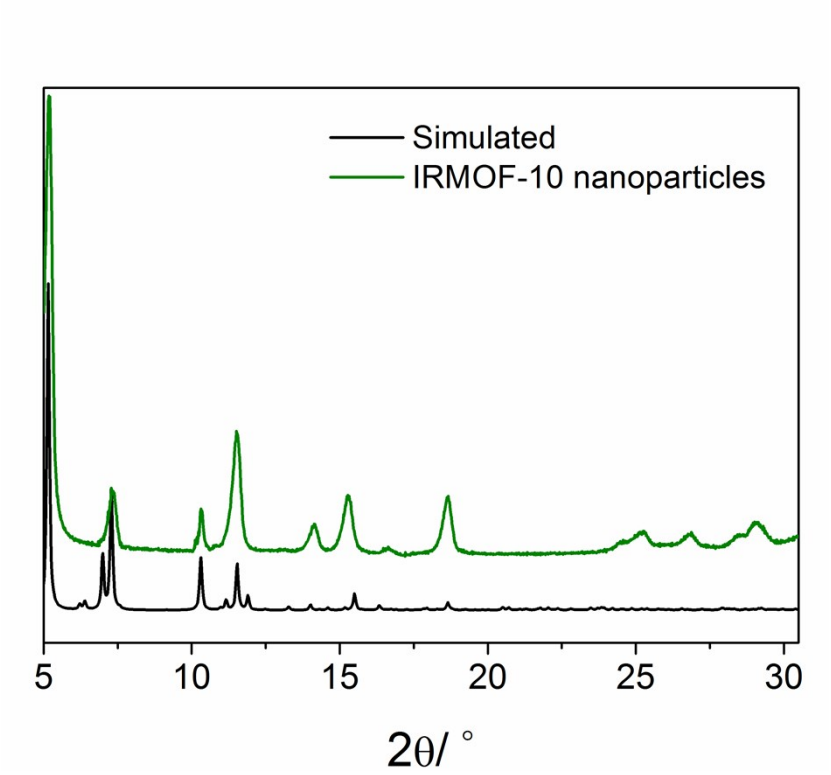

Figure S15. Comparisons of the PXRD patterns of synthesized IRMOF-10 nanoparticles with the simulated diffraction pattern.

Section S6

Fourier Transform infrared spectroscopy (FTIR)

The produced IRMOFs, which were dispersed in ethanol, were centrifuged at 10000 rpm for 15 minutes. The white solids were dried in a vacuum drying oven at room temperature for 12 hours. The dried IRMOF-1, IRMOF-8 and IRMOF-10 solids were mixed with KBr power respectively, and then baked under an infrared lamp to reduce moisture. The dried mixtures were pressed to disks and tested at 25 °C.

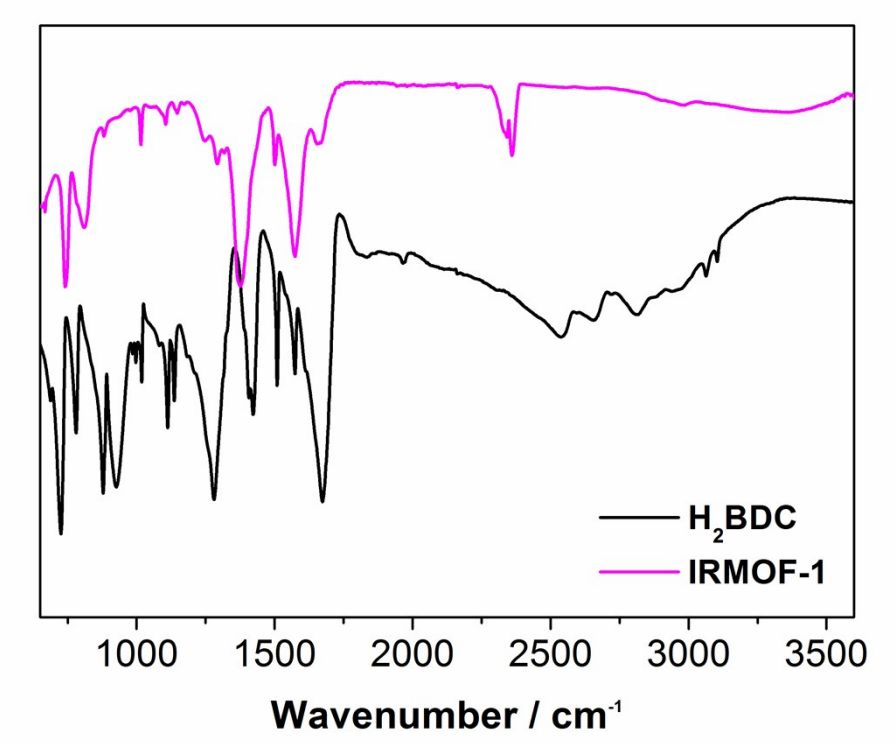

Figure S16. FT-IR spectra of starting material H_2BDC, and the prepared IRMOF-1 nanoparticles.

H_2BDC (3600-650 cm^{-1}): 3103 (w), 3063 (w), 2813 (w), 2657 (w), 2538 (br), 1674 (s), 1574 (w), 1509 (m), 1422 (s), 1407 (s), 1281 (s), 1137 (w), 1112 (m), 1018 (w), 926 (s), 879 (s), 780 (m), 726 (s).

IRMOF-1 (3600-650 cm^{-1}): 3358 (br), 2989 (w), 2100 (w), 2360 (m), 2342 (m), 1660 (m), 1574 (s), 1500 (m), 1375 (s), 1317 (w), 1292 (w), 1247 (w), 1172 (w), 1147 (w), 1105 (w), 1015 (w), 882 (w), 810 (s), 742 (s).

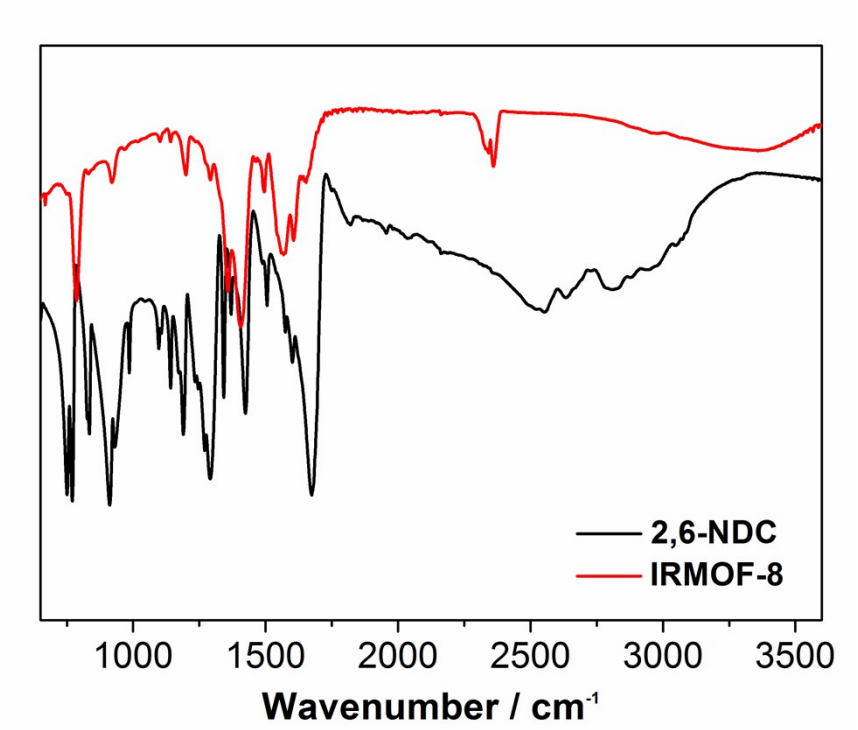

Figure S17. FT-IR spectra of starting material 2,6-NDC, and the prepared IRMOF-8 nanoparticles.

2,6-NDC (3600-650 cm^{-1}): 2807 (w), 2633 (w), 2553 (br), 1674 (s), 1505 (w), 1423 (m), 1342 (m), 1291 (s), 1189 (w), 1141 (w), 1097 (w), 985 (w), 930 (m), 911 (s), 835 (m), 770 (s), 750 (s).

IRMOF-8 (3600-650 cm^{-1}): 3363 (br), 2982 (w), 2360 (m), 2342 (m), 1654 (w), 1605 (w), 1570 (s), 1496 (w), 1405 (s), 1357 (s), 1293 (w), 1200 (w), 1140 (w), 1102 (w), 920 (w), 787 (s).

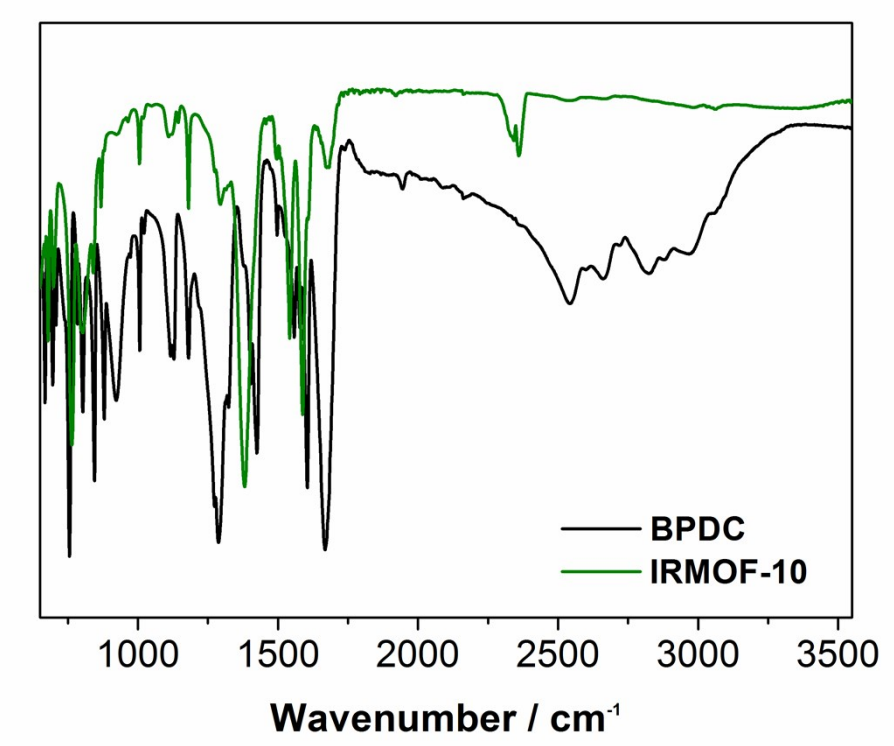

Figure S18. FT-IR spectra of starting material BPDC, and the prepared IRMOF-10 nanoparticles.

BPDC (3600-650 cm^{-1}): 2968 (w), 2824 (w), 2660 (w), 2543 (br), 1667 (s), 1604 (s), 1578 (w), 1558 (w), 1497 (w), 1424 (s), 1287 (s), 1180 (m), 1128 (m), 1116 (m), 1006 (m), 922 (s), 879 (s), 845 (s), 803 (s), 783 (w), 755 (s), 707 (w), 696 (s), 668 (s).

IRMOF-10 (3600-650 cm^{-1}): 3367 (br), 3063 (w), 2984 (w), 2360 (m), 2342 (m), 1675 (w), 1588 (s), 1542 (s), 1381 (s), 1294 (w), 1180 (w), 1110 (w), 1006 (w), 868 (w), 840 (w), 803 (s), 764 (s), 698 (s), 670 (s).

Section S7

N_2 adsorption analysis

The drying and activation of MOF samples were carried out by vacuum heating degassing. After centrifugation, the precipitated sample was put into the degassing station after being dried in the double row tube with the adsorption tube. The heating procedure is set. The temperature is heated at 130 ℃ for 12 hours, and the temperature rise and fall rate is 1 ℃ per minute. At the same time, the vacuum degree of the degassing station is reduced to less than 10 PA. After heating and degassing, the sample was analyzed in BELSORP-max (MicrotracBEL) at 77K.

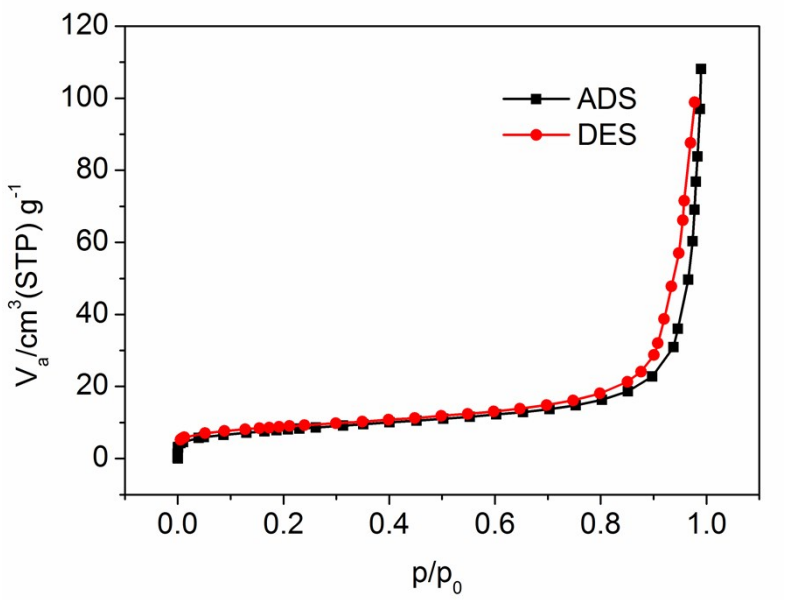

Figure S19. Nitrogen isotherm of IRMOF-1 at 77 K.

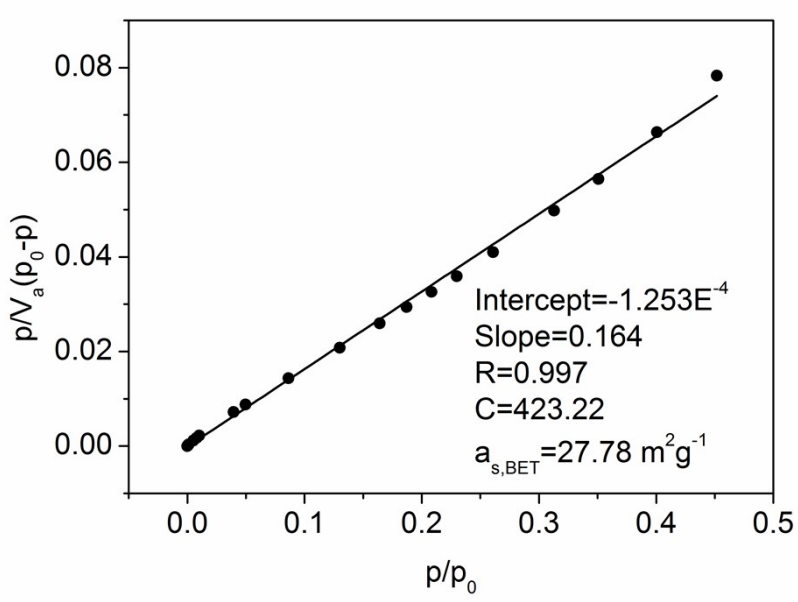

Figure S20. BET area calculation for IRMOF-1 from simulated nitrogen isotherm at 77 K.

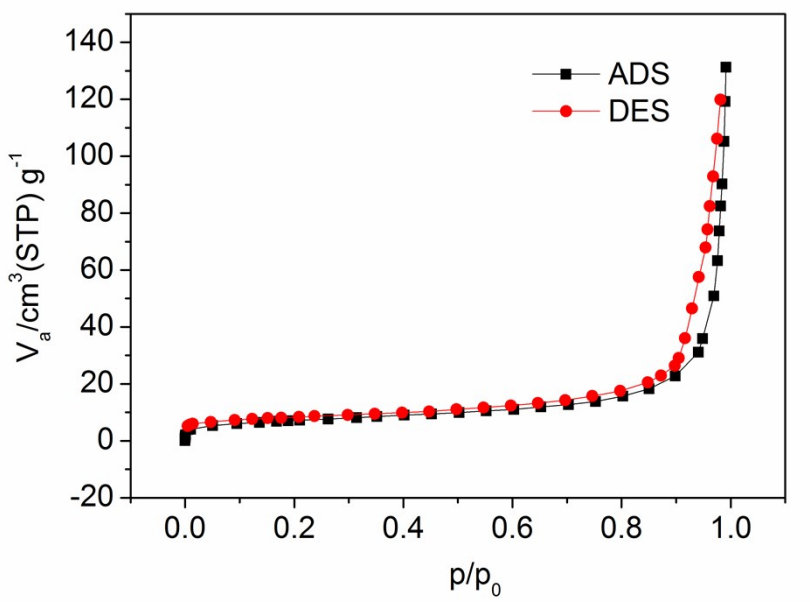

Figure S21. Nitrogen isotherm of IRMOF-8 at 77 K.

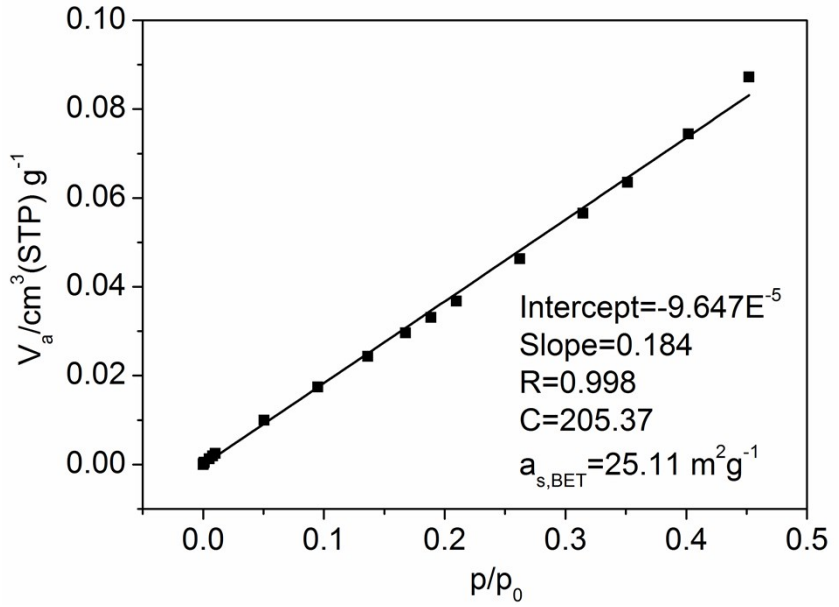

Figure S22. BET area calculation for IRMOF-8 from simulated nitrogen isotherm at 77 K.

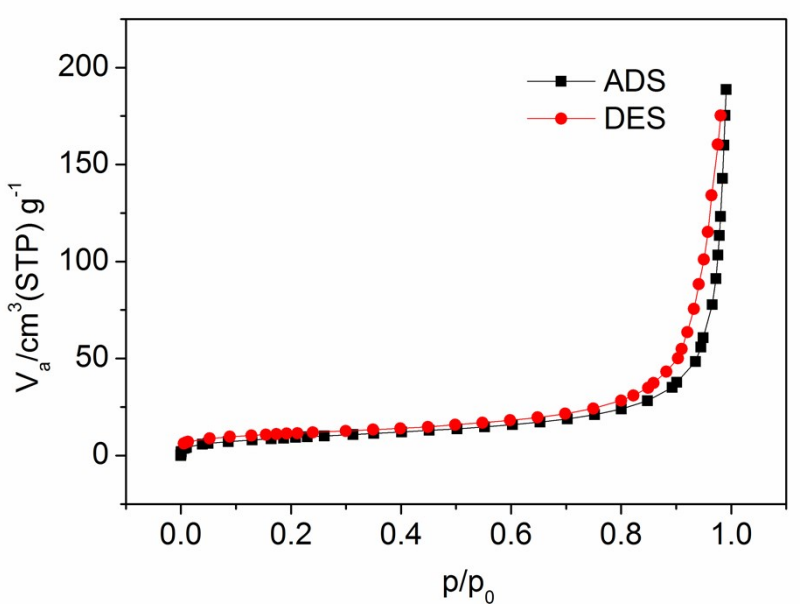

Figure S23. Nitrogen isotherm of IRMOF-10 at 77 K.

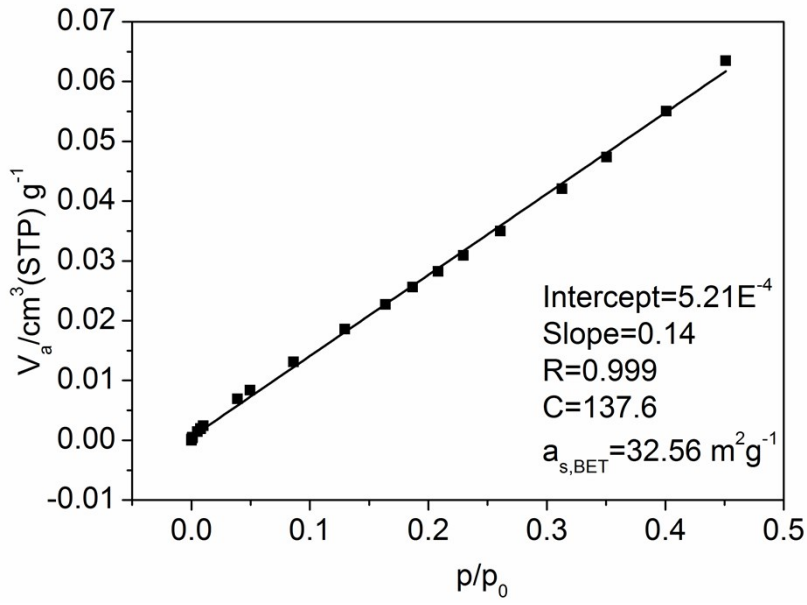

Figure S24. BET area calculation for IRMOF-10 from simulated nitrogen isotherm at 77 K.

Section S8

Quantitatively analyzes the chemical exchange saturation transfer of ^{129}Xe in IRMOFs

The Hyper-CEST effect increases when ^{129}Xe in IRMOF is saturated with RF irradiation under a B_1 field at 3.5, 6.5, 10, 13, and 16 μT.

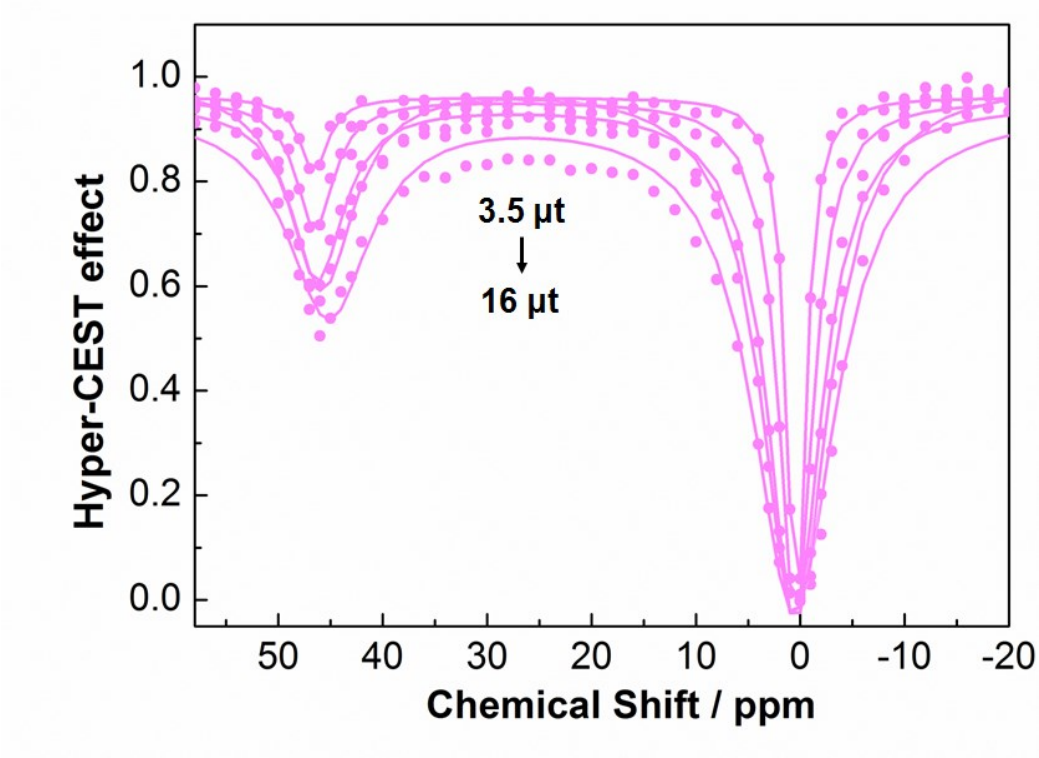

Figure S25. Quantitatively analyzes the chemical exchange saturation transfer of ^{129}Xe in IRMOF-1.

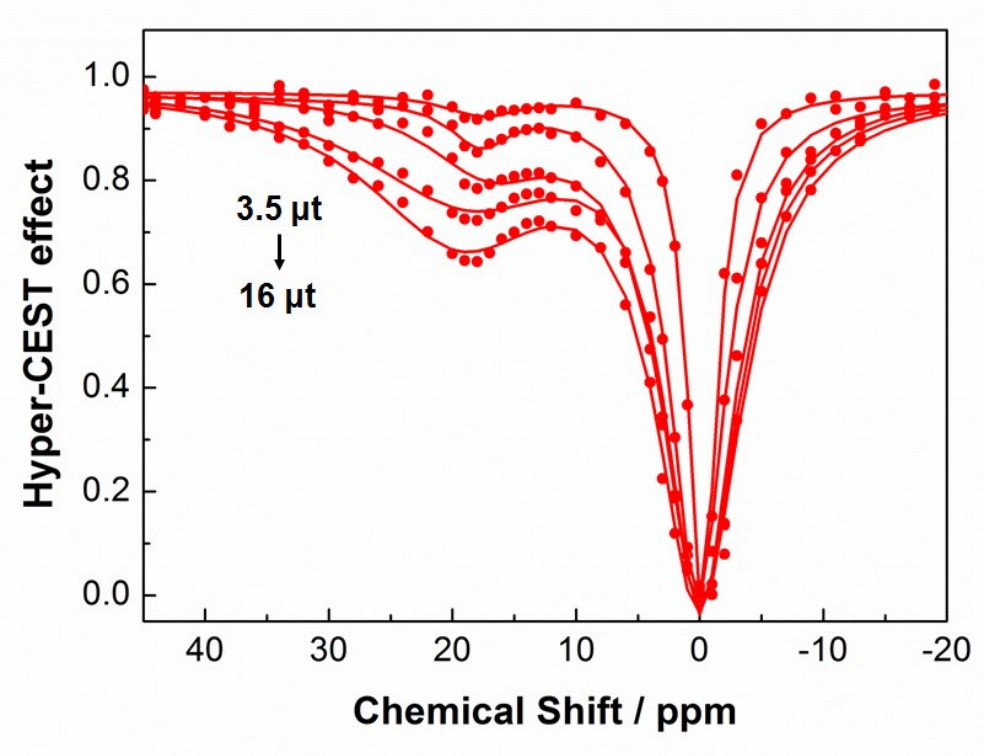

Figure S26. Quantitatively analyzes the chemical exchange saturation transfer of ^{129}Xe in IRMOF-8.

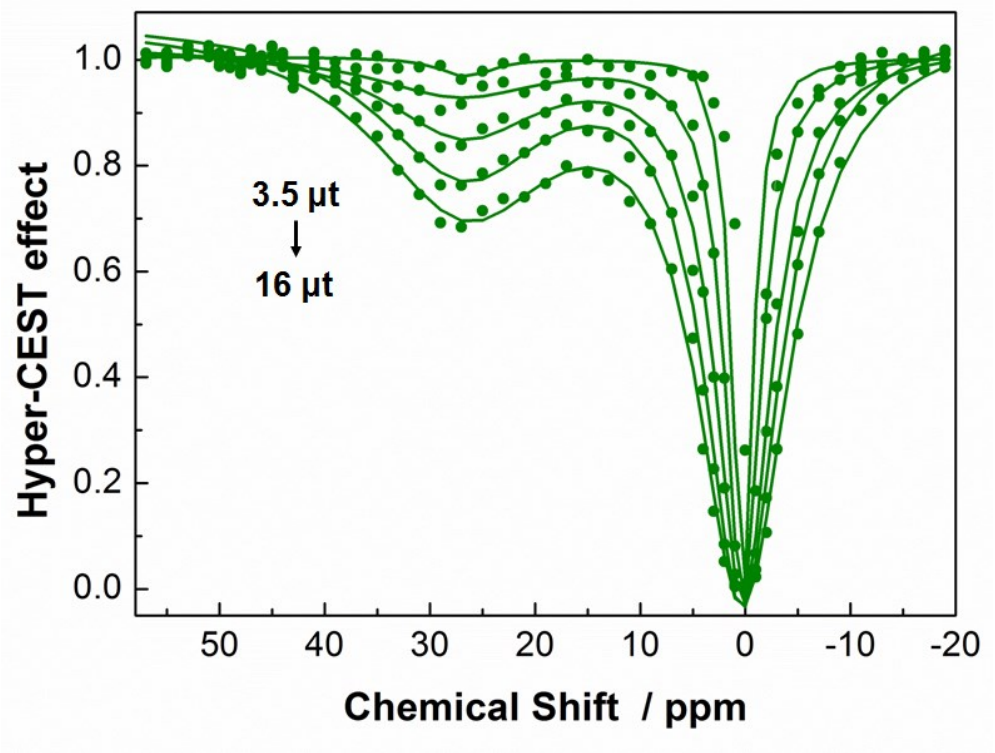

Figure S27. Quantitatively analyzes the chemical exchange saturation transfer of ^{129}Xe in IRMOF-10.

	IRMOF-1	IRMOF-8	IRMOF-10
Free diameter of pores	7.93 Å	9.17 Å	12.15 Å
^{129}Xe exchange rate/ s^{-1}	428.57±152.04	1175.74±936.60	2495.64±547.81
Chemical shift/ ppm	48	17	26

Table S3. ^{129}Xe-host interaction parameters. The free diameter of MOF pores expanded with the extending organic length from IRMOF-1 to IRMOF-10. Meanwhile, the exchange rate of ^{129}Xe atom in MOF increased with the expanding MOF pore diameter.

Section S9

Theoretical Studies

We take one triangle and three edges of one lattice of IRMOF, then put one Xe atom in them, the geometric structure of this are presented in Figure S19. We take R as the distance from Xe to the vertex of the lattice and stretch R along the diagonal line of the lattice to calculate the NMR and the mulliken charge. The NMR and mulliken charge were calculated by wb97XD1 functional and def2-SVP2 basis sets using Gaussian093 software.

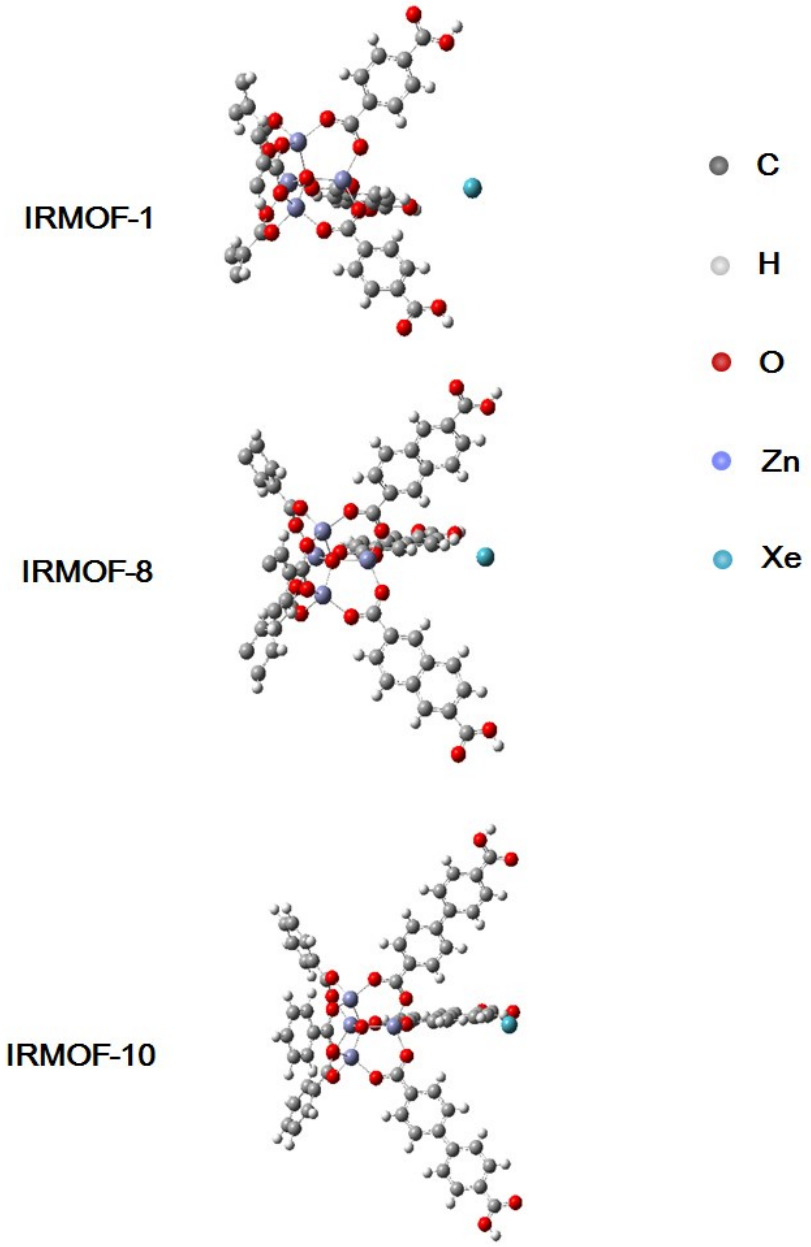

Figure S28. The geometric structures of IRMOF-1, IRMOF-8 and IRMOF-10.

The chemical shift change of three IRMOF systems is shown in Figure S20. Under the same R value, the chemical shift of ^{129}Xe in different IRMOFs is IRMOF-1>IRMOF10>IRMOF-8.

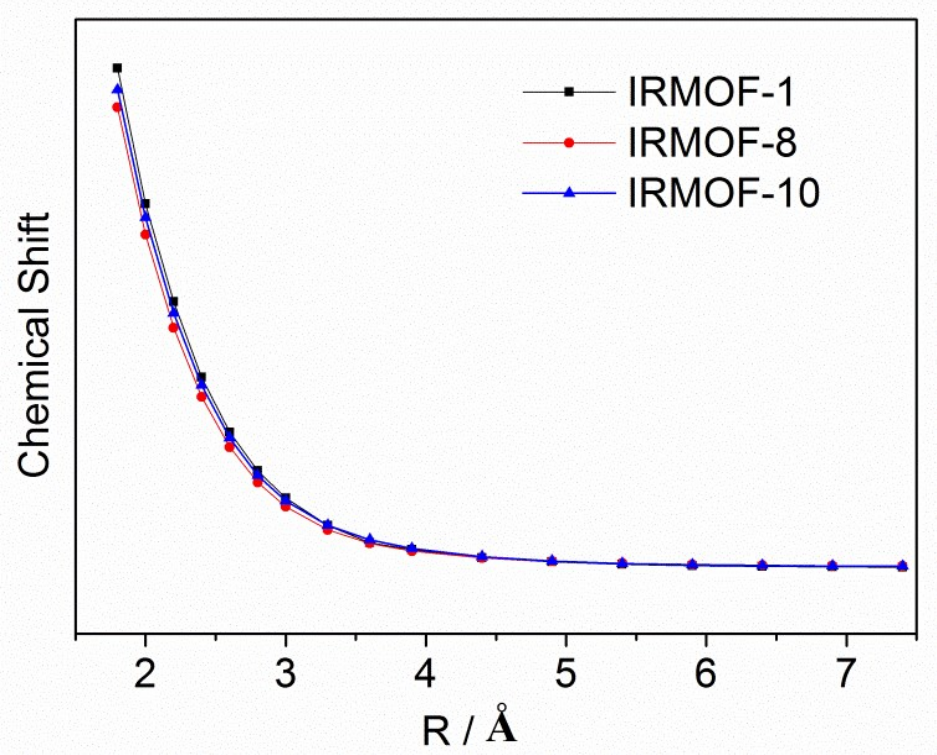

Figure S29. Calculate irradiation frequency difference in IRMOF-1, IRMOF-8 and IRMOF-10.

		Xe	Zn	O	C	H
R=1.8 Å	IRMOF-1	-0.312	1.054	-0.407	0.143	-0.111
	IRMOF-8	-0.295	1.015	-0.362	-	-
	IRMOF-10	-0.294	1.043	-0.400	0.124	-0.080
R=2.4 Å	IRMOF-1	0.017	0.801	-0.437	0.152	-0.124
	IRMOF-8	0.028	0.785	-0.390	-	-
	IRMOF-10	0.024	0.803	-0.428	0.131	-0.093
R=2.8 Å	IRMOF-1	-0.010	0.864	-0.445	0.158	-0.132
	IRMOF-8	-0.011	0.857	-0.398	-	-
	IRMOF-10	0.009	0.839	-0.436	0.137	-0.100

Table S4. Chemical shift difference relates to the charge change of MOF. The charge of IRMOF-1, IRMOF-8, and IRMOF-10 with *R* =1.8, 2.4, and 2.8 Å.

References

1. Z. Zhang, Y. Chen, X. Xu, J. Zhang, G. Xiang, W. He, X. Wang, Well-Defined Metal–Organic Framework Hollow Nanocages, *Angew. Chem. Int. Ed.* **2014**, 53, 429 –433.
2. M. Bosch, S. Yuan, W. Rutledge, H. Zhou, Stepwise Synthesis of Metal–Organic Frameworks, *Acc. Chem. Res.* **2017**, 50, 857−865.
3. L. He, Y. Liu, J. Liu, Y. Xiong, J. Zheng, Y. Liu, Z. Tang, Core–Shell Noble-Metal@Metal-Organic-Framework Nanoparticles with Highly Selective Sensing Property, *Angew. Chem. Int. Ed.* **2013**, 52, 3741-3745.
4. Y. Tan and H. Zeng, Self-templating synthesis of hollow spheres of MOFs and their derived nanostructures, *Chem. Commun.* **2016**, 52, 11591-11594.
5. M. Eddaoudi, J. Kim, N. Rosi, D. Vodak, J. Wachter, M. O'Keeffe, O. M. Yaghi, Systematic Design of Pore Size and Functionality in Isoreticular MOFs and Their Application in Methane Storage, *Science* **2002**, 295, 469-472.